

INFN/AE - 67/7
20 Giugno 1967

A γ -RAY DETECTOR FOR THE STUDY OF THE

ELECTROMAGNETIC DECAY OF RESONANCES

F. Bradamante^{*)}, G. Fidecaro^{**†)}, M. Fidecaro^{†)},
M. Giorgi^{*)}, F. Sauli^{*)}, and P. Schiavon^{*)}.

20 June 1967

†) CERN, Geneva, Switzerland.

*) Istituto di Fisica della Università, Trieste, Italy.
Istituto Nazionale di Fisica Nucleare, Sottosezione di Trieste, Italy.

/968/5
p/sm

Summary

A large size gamma ray detector made of eleven thin plate optical spark chambers alternated with lead plates has been constructed and used to search for $\rho^- \rightarrow \pi^- \gamma$ decay. The detection efficiency is close to 100% down to an energy as low as 30 MeV. The conversion point of a shower is reconstructed with an accuracy of a few mm.

A total of $2.4 \cdot 10^4$ pictures of showers from $p\pi^- \pi^0$ events has been recorded.

1. INTRODUCTION

Since the spark chamber was introduced into the study of high-energy phenomena, various experimentalists have tried to extend its use to the detection of γ -rays. Efficient γ -ray detectors were built, for example, for the study of pion-nucleon charge-exchange scattering at high energy.

We became interested in spark chamber γ -ray detectors in 1963, when we started a study of the electromagnetic decay of resonances and in particular a search for the $\rho \rightarrow \pi\gamma$ decay. In the more recent years we have been encouraged to continue along this line of research by the fact that the electromagnetic decay of resonances has been recognized to be very interesting for the understanding of the part played by the resonances in the various symmetry schemes¹⁾.

We would like to report in the following about the γ -ray detector we built at the NP Division of CERN to search for the $\rho \rightarrow \pi\gamma$ decay²⁾. At the time of the choice of the most convenient detector we came to the conclusion that a large-size high angular resolving power γ -ray detector, based on the use of spark chambers, would have made possible a wide range of experiments in the field of electromagnetic decay of resonances. Our recent experience has confirmed this point of view so that we are now designing a new detector of even larger size, working on the same principle, which will make use of magnetostrictive wire spark chambers.

2. THE γ -RAY DETECTOR

Figure 1 shows the apparatus used for the study of the $\rho \rightarrow \pi\gamma$ decay²⁾. The γ -ray detector is visible on the left. It consists of eleven thin plate optical spark chambers alternated with an equal number of lead conversion plates. Every chamber has four 8 mm gaps in which the electron shower produced in the earlier lead plates is detected. The thickness of the lead plates was chosen, as it will be discussed below, equal to 3 mm; this gives a total of 6.5 radiation lengths of lead,

corresponding to an asymptotic conversion probability for high energy γ -rays of 98.9%. The lead plates, not being part of the chambers, could easily be replaced with other material if this was required.

In order to get the highest possible efficiency for the detection of low energy γ -rays (~ 30 MeV), even in the presence of several other sparks, each spark chamber was built with four gaps, and not with the two gaps strictly necessary. Moreover, the thickness of the lead plates was maximized by means of a Monte Carlo calculation³⁾. The results of the Monte Carlo calculation are shown in Figs. 2, 3, 4. Figure 2 gives the detection inefficiency for a 3 mm lead plate as a function of the γ -ray energy, i.e. the probability that no charged particle comes out of the plate if a γ -ray has interacted in it. Figure 3 gives the total inefficiency of our set-up, i.e. the probability of not "seeing" at all γ -rays of given energy. The second curve of Fig. 3 is the probability of the primary γ -ray not interacting in the whole system of lead plates; for primary energies larger than 100 MeV the two curves practically coincide. Figure 4 shows, for the particular energy of 30 MeV, as a function of the thickness of the lead plates:

- a) the detection inefficiency (i.e. the probability of not seeing a γ -ray which interacted in one of the eleven plates);
- b) the probability of a γ -ray not interacting in the chamber;
- c) the combination of curves (a) and (b), which gives the inefficiency of the chamber in seeing γ -rays; the further conversion of the secondary γ -rays of the electron showers is not taken into account;
- d) the effect of the conversion of the secondary γ -rays;
- e) the total inefficiency of the chamber.

It can be seen that there is a flat minimum in the region around 3 mm. It should also be noticed that the increase in efficiency due to the conversion of secondary γ -rays is small. This is important because if no primary γ -ray is visible in the chamber and the measure-

ments are done on a secondary γ -ray, moves in the direction can be introduced. In fact, in the case of low energy the secondary γ -rays tend to deviate away from the direction of the primary γ -rays.

3. SPARK CHAMBERS

Each one of the independent spark chambers, which form the detector, was made, as shown in Fig. 5, of five parallel hardened aluminium plates 0.025 mm thick; two 0.19 mm mylar walls ensured the tightness of the chamber. The technique used to build the spark chambers was similar to the one developed by Meyer and Terwilliger⁴⁾.

The aluminium foil was glued on a 50 mm wide, 8 mm thick, square plexiglas frame, in the following way. The frame, cooled at about 3°C and coated with Eastman 150 glue^{*)}, was pressed for a few seconds on the aluminium foil laid down on a glass plate at room temperature. When the frame reached the room temperature the aluminium foil became well stretched and flat. The technique was improved by predeforming the frames by means of forces applied perpendicularly at the centre of the four sides. The six frames were then stuck together with Araldite^{**)}.

The 3 mm thick lead^{***)} plate, was glued with Araldite to a steel frame, which acted as a support.

As visible in Fig. 1 the chambers had different useful dimensions, the largest being 95 x 95 cm². A 2.5 x 6.5 cm² hole in the lead plates allowed the beam to go through, in order to minimize beam interactions. The eleven chambers and the lead plates were held together by clamps.

Each aluminium foil had an external tab, which was alternately connected to ground or to the HV pulser; the outer electrodes of the chamber were always grounded.

*) Eastman Kodak Co. Produc. and Armstrong Co. Industrial Division Distrib., Lancaster, U.S.A.

***) Araldite, No. 106, CIBA, Basle, Switzerland.

***) Containing a small percentage of antimonium to have more rigidity.

A 2.6 kV negative pulse, 40 nsec wide at the base, was applied to the master spark gap through an EL 360 tube driven by an EFP 60 (Fig. 6). The 10 kV output pulse triggered a set of similar secondary spark gaps, mounted directly on each one of the eleven spark chambers (Fig. 7), in order to minimize the total series inductance. As a result, a 10 kV pulse was applied to the HV electrodes of the chambers, with a rise-time of about 50 nsec. The largest chambers had a capacity of ~ 1000 pF per gap, resulting in 4000 pF for each element; the discharging condensers fixed on the secondary spark gap had a capacity of 14,000 pF. The total delay between the passage of the particles and the application of the HV pulse to the spark chambers was about 300 nsec, including the delays of the cables. The delay introduced by the two hard tubes was 55 nsec and the delay introduced by the main and the secondary spark gaps was estimated to be about 15 nsec.

A clearing field of ~ 60 V/cm was also applied to each gap, opposite in direction to the HV pulse.

Each element of the spark chamber system was connected to the gas circuit through an inlet and an outlet hole drilled in the plexiglas wall. A commercial mixture of Ne-He (Henogal, 70% Ne and 30% He) was used; the gas was allowed to circulate in a closed circuit (Fig. 8) and was purified by passing through a calcium oven at 600°C . A gasometer, filled automatically from the gas cylinder, provided the system with a constant pressure of about 2 mm of water above the atmospheric pressure. The chambers were washed before use by means of a flux of helium. With these particular conditions of filling and with the value of the clearing field mentioned above, the chamber memory was of 700 nsec (half clearing time), in agreement with the percentage of double tracks observed in the beam chambers during the experiment (2.3% for 1.3×10^5 incoming particles).

4. OPTICS

Pictures were taken from two views; one direct, the other at 90° through reflection on a 45° mirror. In both cases a plexiglas field lens, 1.4 m diameter, was utilized. Each lens had a radius of curvature of 5 m and was carved at the main CERN workshop from 7 cm thick plexiglas plate^{*)}. The details of the optics will be given elsewhere.

The two home-made cameras could take one picture per PS burst; they could store 120 m of 35 mm film.

Each camera was placed at the focal point of the spherical field lens (10.85 m ahead of it) so that the angles measured on the film gave directly the projected angles of the track.

The inherent spherical aberrations were very small. They were corrected by the general computer programme used for the reconstruction of the events. The objectives of the cameras were Componons^{**)}, 1:5.6 aperture, and 210 mm focal length. With this aperture the diameter of the circle of confusion corresponding to the centre of the detector was about 1.4 mm in the direct view and 3 mm for the indirect view (for this view the camera was focussed in such a way to have a confusion circle of ~ 0.7 mm on the reference reticule).

Kodak Linograph Pan film was used which could resolve lines 20 microns apart; this corresponds to 1 mm in real space.

Since we used, in the same set-up, spark chambers of different dimensions, it was necessary to equalize the luminosity of the sparks. This was obtained by placing neutral absorbing glass of appropriate thickness in front of the various spark chambers of the γ -detector. An aperture of f/11 for the objectives gave the best results.

*) Because of the large dimensions needed, two 7 cm thick plates had to be glued together using Tensol, I.C.I., Herts., England.

***) Jos. Schneider and Co. Optische Werke, Kreuznach/Rhld., Germany.

5. PERFORMANCE

Because of the particular design, the efficiency for the detection of γ -rays was not affected critically by the efficiency of the single gaps. This fact allowed us to operate the detector successfully even if some chamber showed the usual tendency for a spark to rob energy from the electrically adjacent gap. However, we verified that the efficiency of the single gaps for single particles in the absence of robbing effects was practically 100% and that the over-all efficiency remained stable in time.

The multispark efficiency of the system was tested by counting the total number of sparks which formed the track of a π^- meson in the presence of zero, one or two γ -rays. The results are shown in Table 1.

The data have been grouped in two categories according to the angle of inclination of the track α . The efficiency reported is the effective efficiency observed.

Table 1

Inclination of the track	0 " γ "	1 " γ "	2 " γ "
$0 < \alpha < 10^\circ$	91.3	81.5	74.0
$10 < \alpha < 20^\circ$	91.0	81.1	72.0

Concerning the efficiency of the γ -ray detector as a function of the energy, a comparison between the observed energy spectrum of the γ -rays obtained from the kinematical reconstruction of $p\pi^-\pi^0$ events, and the expected spectrum, computed by means of a Monte Carlo method, has been made and reported in Fig. 9. One can conclude that in the limit of the experimental errors the efficiency is in agreement with the results of the calculations reported in Section 2.

Concerning the accuracy in the reconstruction of the γ -rays, because the straight line through the vertex of the reaction and the conversion point was taken as a direction of the γ -rays, the precision was limited by the small distance of the γ -ray detector from the hydrogen target (see Fig. 1). Thus the precision was fixed essentially by the error in the location of the conversion point. This error was evaluated in various ways:

- 1) A few events, representing different configurations, were measured 50 times.
- 2) Several events were measured twice, and the distribution of the differences between the first and the second measurements was analysed.
- 3) A distribution of the differences of the coordinates perpendicular to the chambers measured in both views was made.

Everything was found consistent with an uncertainty in defining the conversion point of ± 3 mm for the two coordinates in the xy plane parallel to the chambers, and of ± 5 mm for the z coordinate perpendicular to the chambers. This lead to an error in the angle of less than 0.4° .

No attempt was made to compare the direction of the γ -rays determined as explained above with the axis of the shower, although in the case of a high energy γ -ray the shower was so narrow as to look like a single charged particle. This study can be more conveniently executed with the new detector we intend to build which, because of its digital output, will allow one more easily to compute the direction of the axis of the shower also for low energy γ -rays.

The distribution of the point of origin of the showers along the direction of the γ -ray has also been checked. It shows the correct exponential behaviour.

Some typical events with one γ -ray and two γ -rays can be seen in Fig. 10.

No attempt to determine the energy of a γ -ray from the total number of sparks has been made as the total thickness of lead was not sufficient to absorb the whole shower. In fact, for a 2 GeV γ -ray the end of the apparatus corresponds to the position of the maximum development of the shower.

6. ACKNOWLEDGEMENTS

Messrs. P. Dechelette and M. Renevey took care of the construction of the chambers. Miss H. Orwat was responsible for the scanning. We thank Professors W. Paul and P. Preiswerk for the kind hospitality some of us have received at the CERN laboratories.

REFERENCES

- 1) L.D. Soloviev, Symmetries and current algebras for electromagnetic interactions, Talk at the International Conference on Low and Intermediate Energy Electromagnetic Interactions, Dubna, Feb. 7-15, 1967.
- 2) G. Fidecaro, M. Fidecaro, J. Poirier, P. Schiavon, Physics Letters 23, 163 (1966).
- 3) F. Bradamante, A Monte Carlo calculation for the efficiency of the γ -ray detection chamber in the $\rho \rightarrow \pi\gamma$ experiment. CERN Int. Rep. NP/8855/k1, May 1964.
- 4) D.I. Meyer and K.M. Terwilliger, Rev.Scient.Instr. 32, 512, 1961.

Figure Captions

- Fig. 1 The experimental apparatus used to search for the $\rho \rightarrow \pi\gamma$ decay mode.
- Fig. 2 The detection efficiency for a 3 mm Pb plate as a function of the γ -ray energy.
- Fig. 3 The total inefficiency of the γ -ray detector (does not include the electronic inefficiency) and the probability of a γ -ray not interacting in the lead plates.
- Fig. 4 The various efficiency curves for the γ -ray detector at 30 MeV. Each curve is discussed in the text.
- Fig. 5 Exploded vertical cross-section of one of the 11 modules which constitute the γ -ray detector. The plexiglas bands are 8 mm thick and 50 mm wide.
- Fig. 6 The spark gap.
- Fig. 7 Electrical details of a spark chamber.
- Fig. 8 Diagram of the gas circuit.
- Fig. 9 The γ -ray energy spectrum for $p\pi^-\pi^0$ events: a) experimental b) computed by results of a Monte Carlo computer program.
- Fig. 10a) A typical one- γ event ($\pi^- p \rightarrow p\pi^-\gamma$)
 b) A typical two- γ event ($\pi^- p \rightarrow p\pi^-\pi^0$).

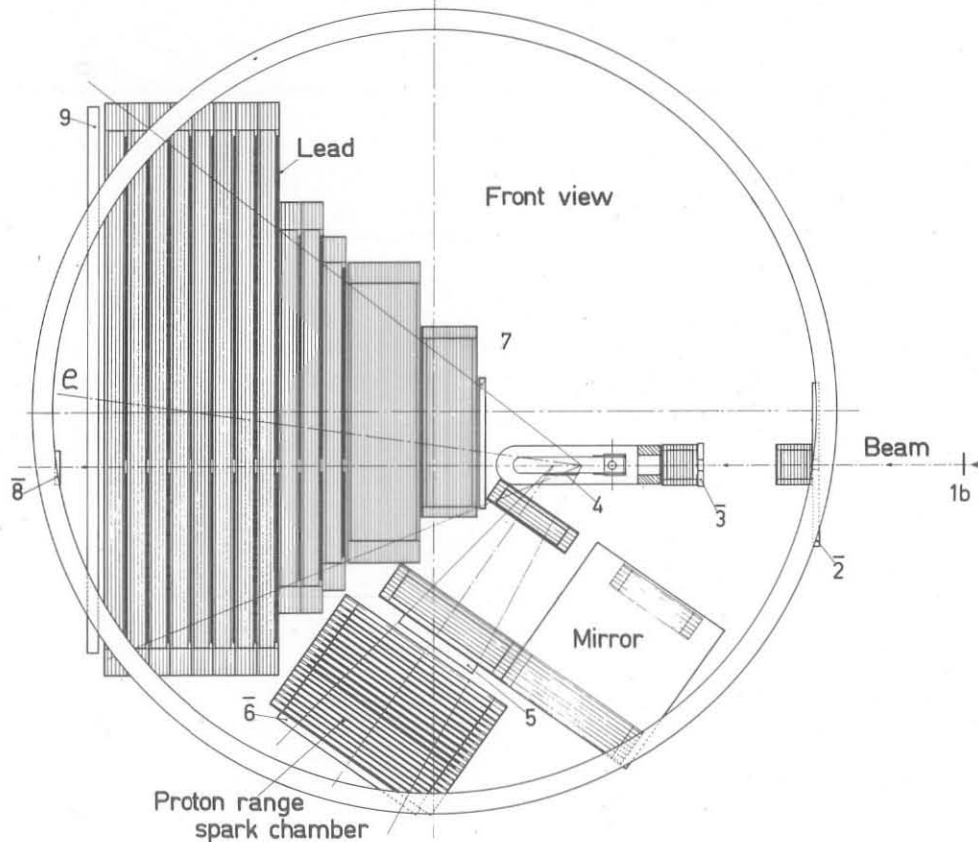
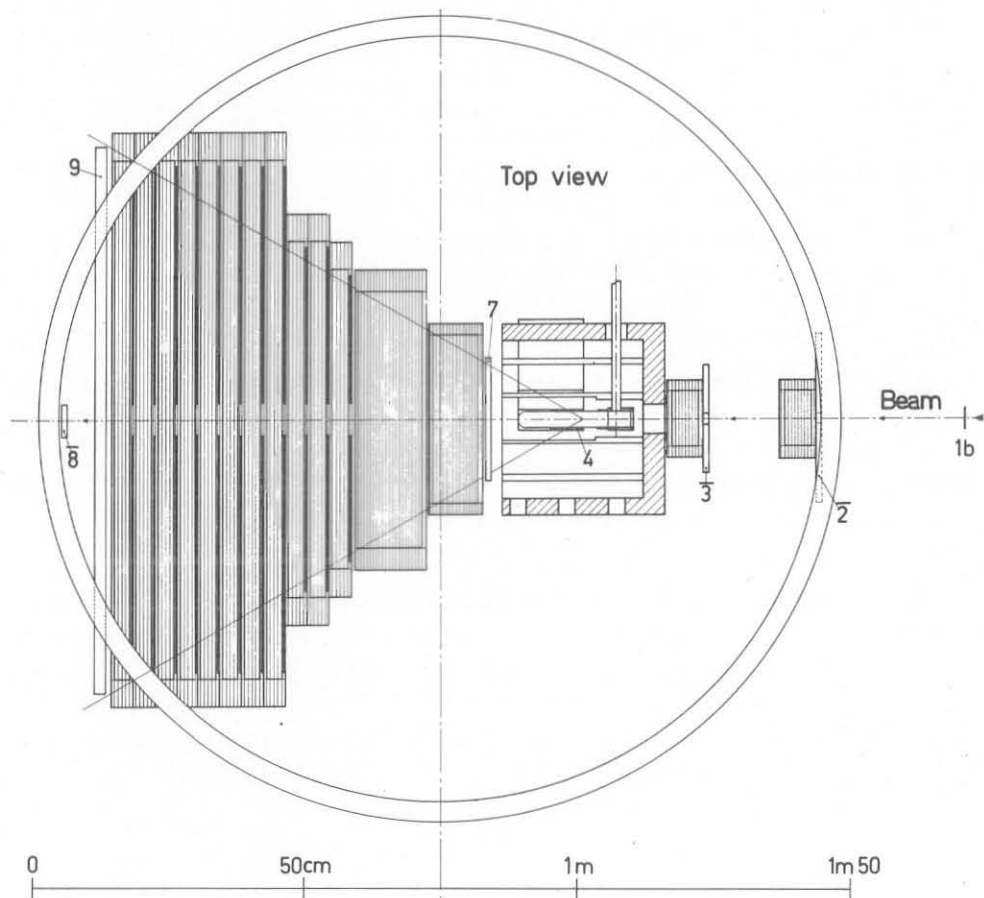


FIG. 1

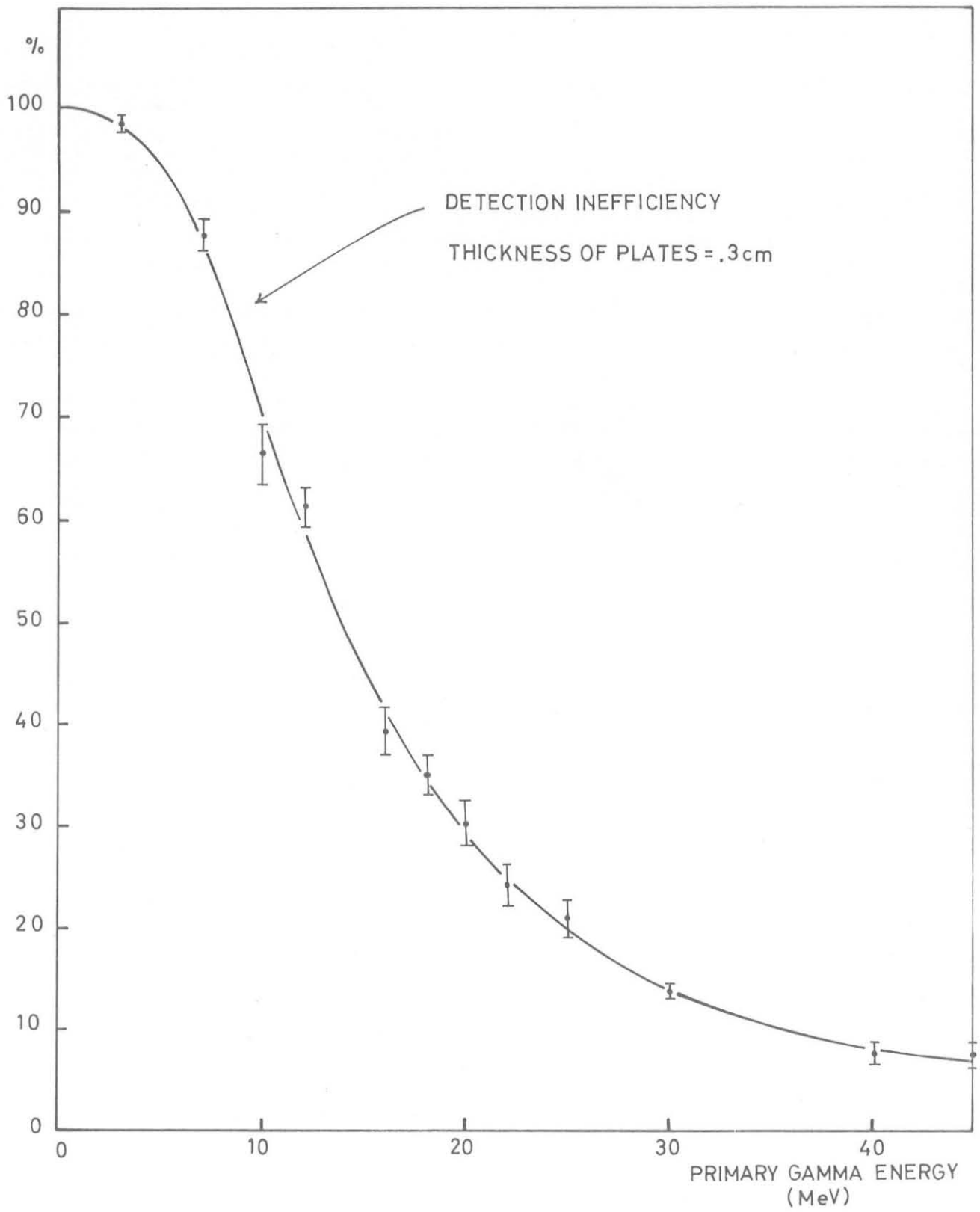


FIG. 2

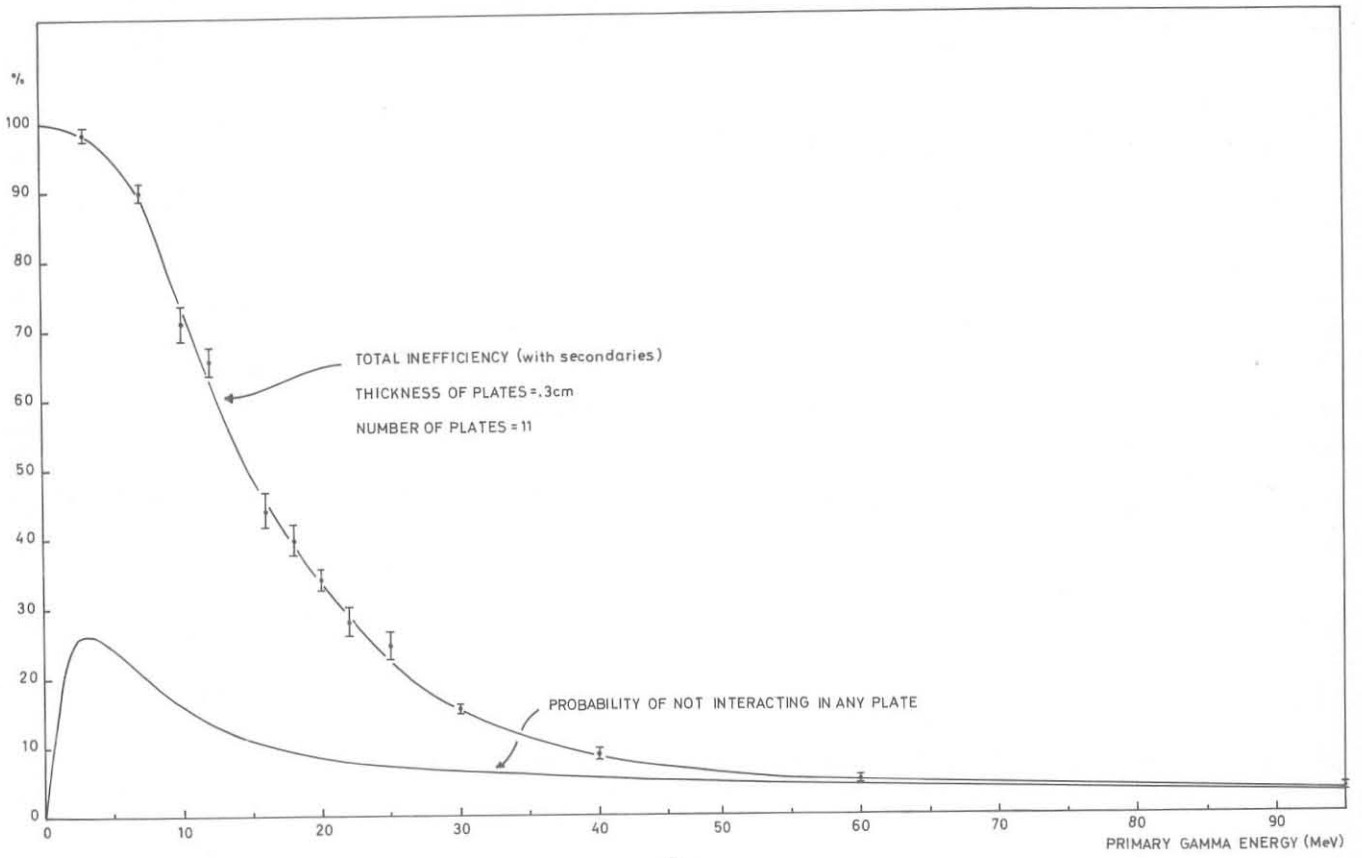


FIG. 3

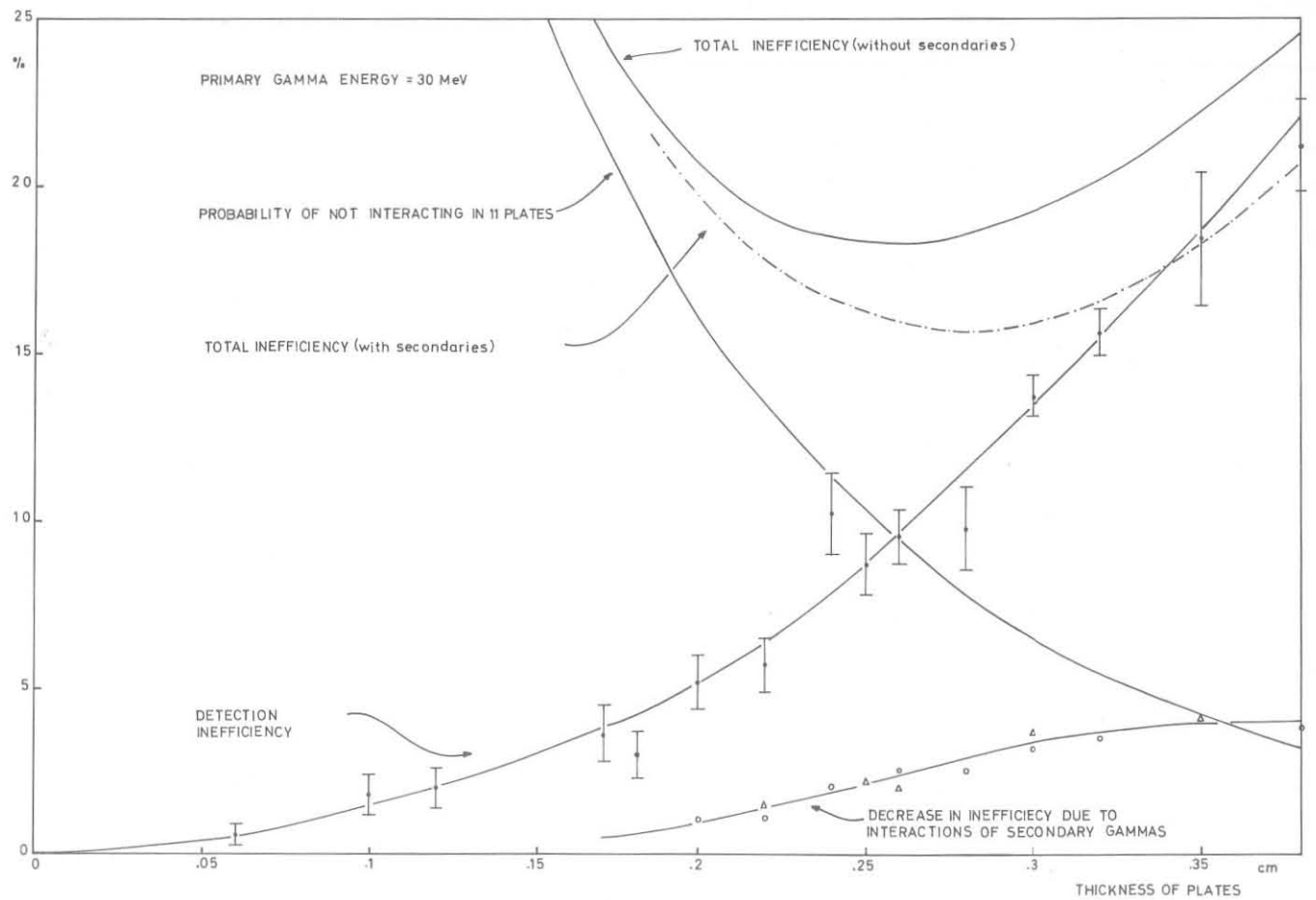


FIG. 4

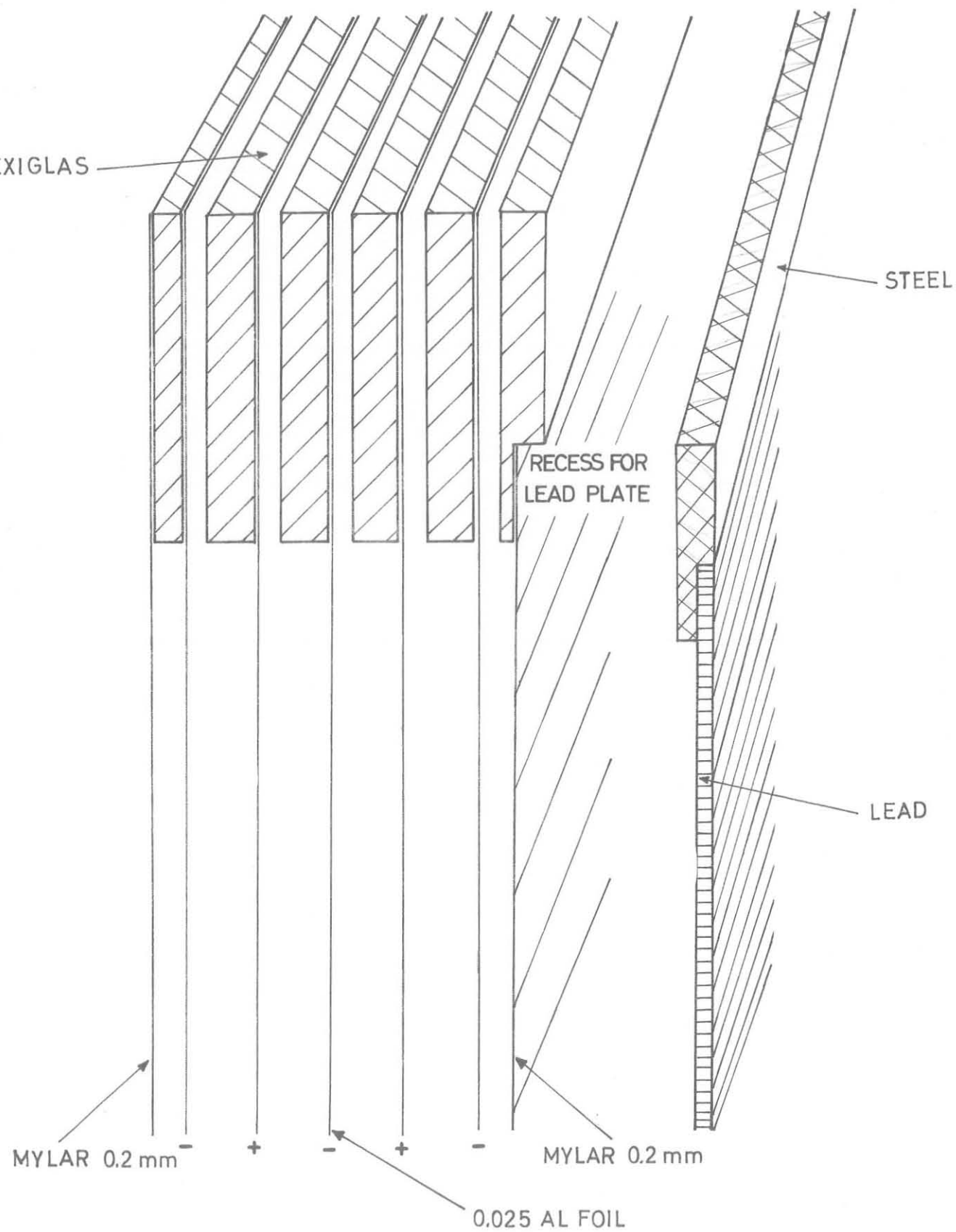
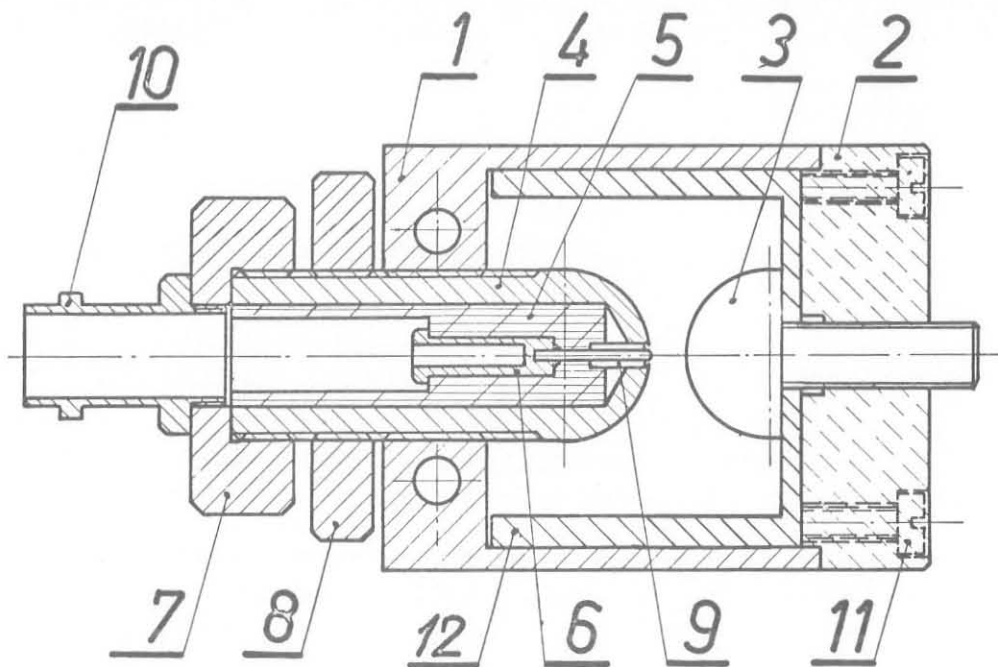


FIG. 5



- 1 Spark box
- 2 Electrode support (plexiglas)
- 3 Electrode (inox)
- 4 Electrode (inox)
- 5 Insulator (teflon)
- 6 Electrode
- 7 Adjusting nut
- 8 Blocking nut
- 9 Insulating tube (porcelain)
- 10 H.V. BNC Connector
- 11 Screw (nylon)
- 12 Insulating cylinder (plexiglas)

Fig.6

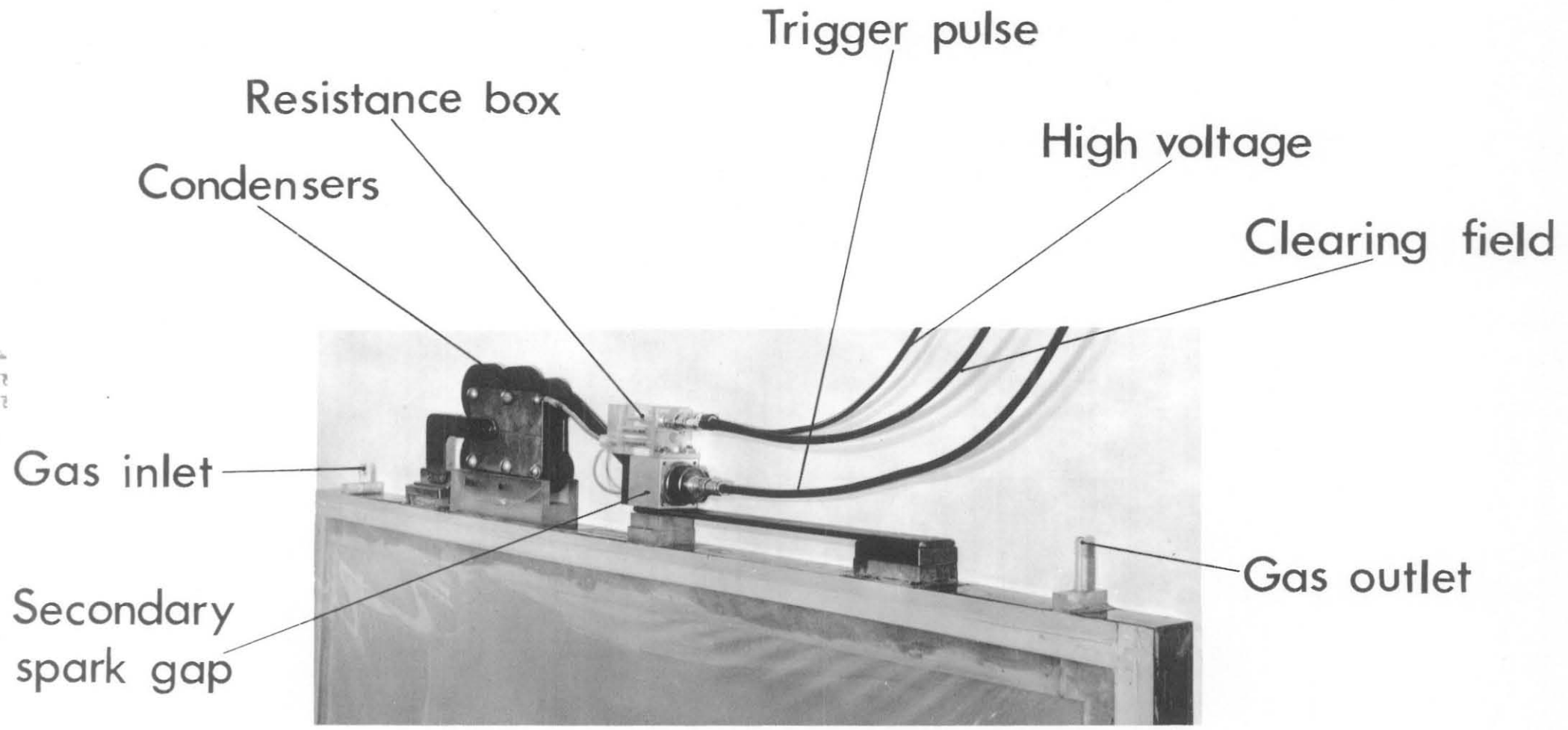
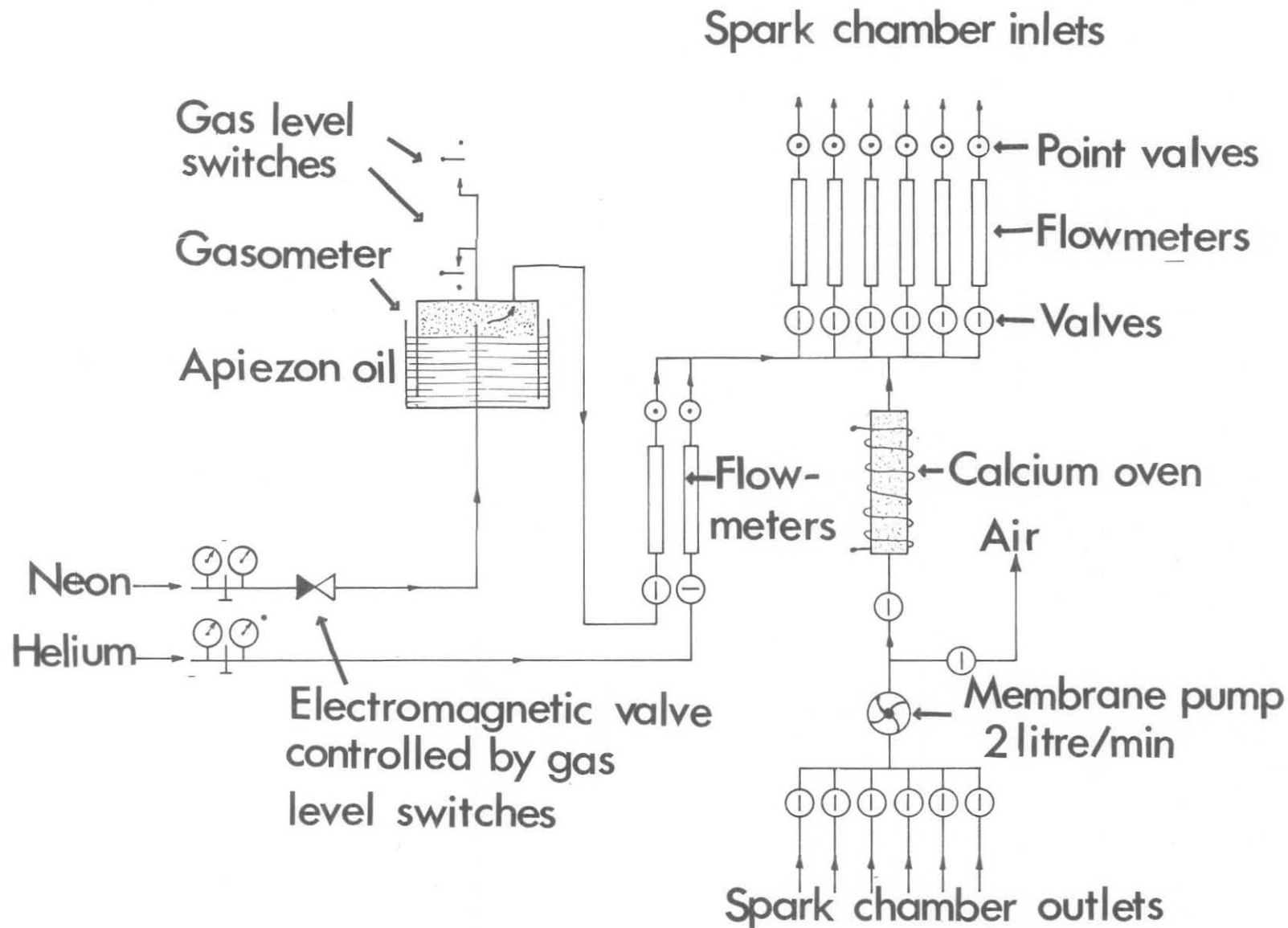


Fig.7



SPARK CHAMBER GAS SUPPLY

Fig.8

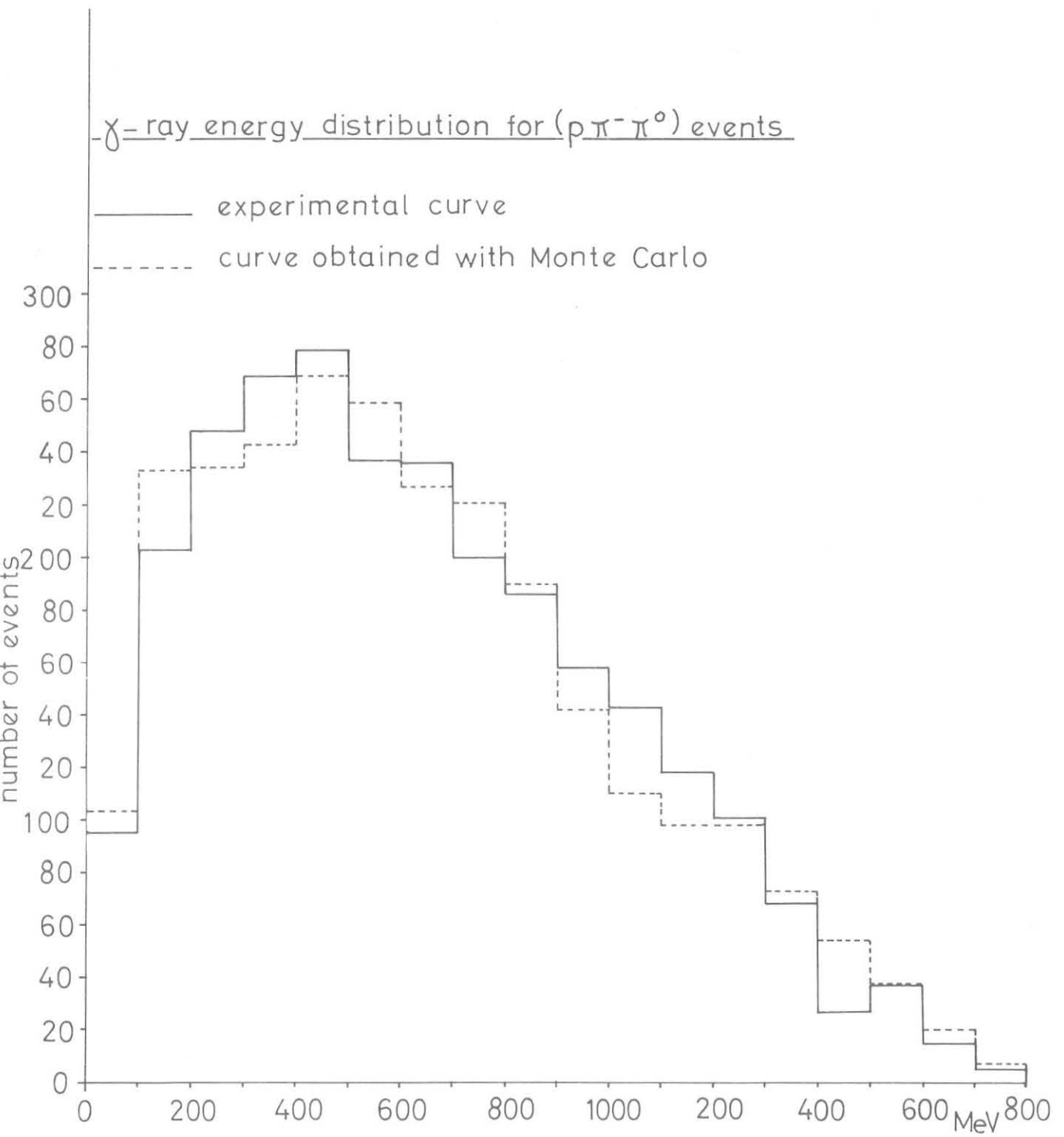


Fig.9

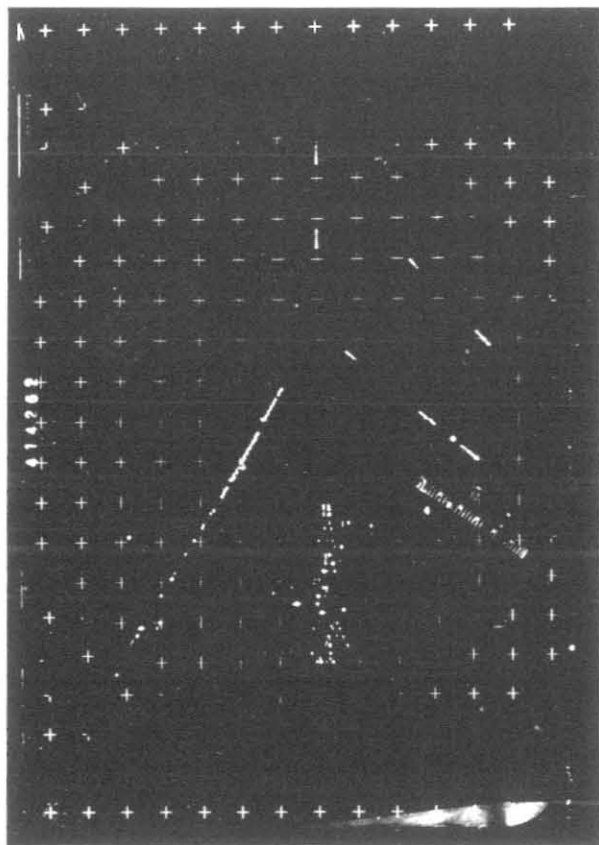
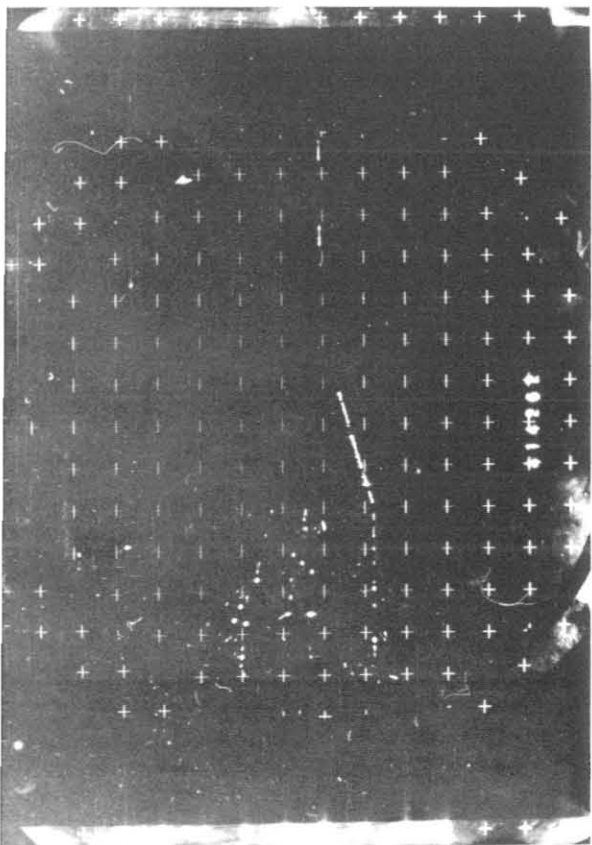


Fig. 10b

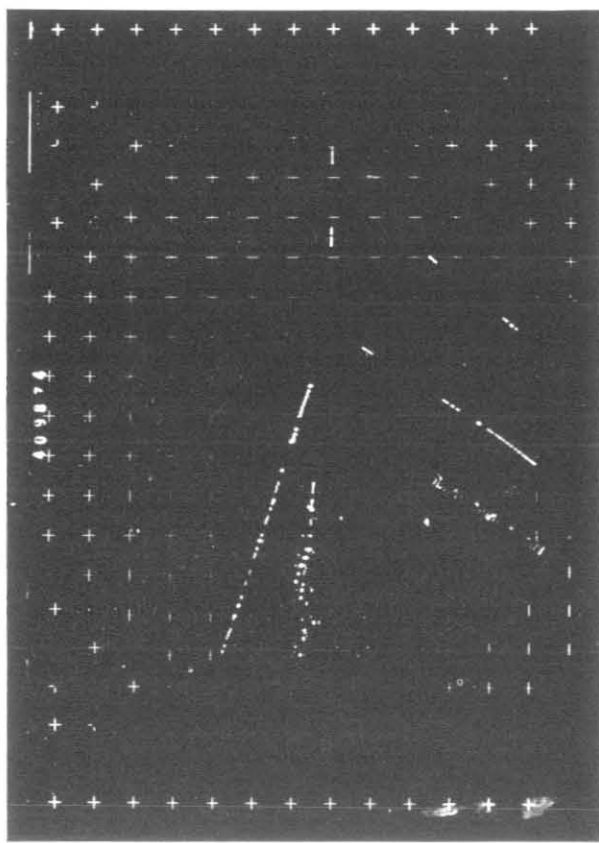
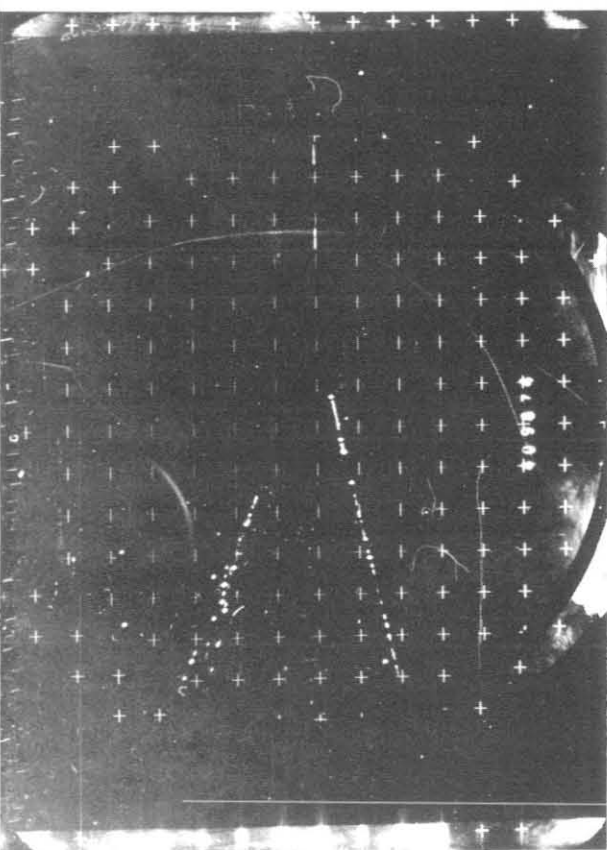


Fig. 10a